Original Investigation

Noninvasively Evaluating the Grading of Glioma by Multiparametric Magnetic Resonance Imaging

Lei Zhang, Master of medicine[1], Liu-qing Yang, Bachelor of medicine[1], Li Wen, MD, Sheng-qing Lv, MD, Jun-hao Hu, Master of medicine, Qing-rui Li, Master of medicine, Jian-ping Xu, MD, Ru-fu Xu, MD, Dong Zhang, MD

Rationale and Objective: To investigate the performance of multi-parametric magnetic resonance imaging (MRI) for glioma grading.

Materials and Methods: Seventy consecutive patients with histopathologically confirmed glioma were retrospectively evaluated by conventional MRI, dynamic susceptibility-weighted contrast-enhanced, multiple diffusion-weighted imaging signal models including mono-exponential, bi-exponential, stretched exponential, and diffusion kurtosis imaging. One-way analysis of variance and independent-samples *t* test were used to compare the MR parameter values between low and high grades as well as among all grades of glioma. Receiver operating characteristic analysis, Spearman's correlation analysis, and binary logistic regression analysis were used to assess their diagnostic performance.

Results: The diagnostic performance (the optimal thresholds, area under the receiver operating characteristic curve, sensitivity, and specificity) was achieved with normalized relative cerebral blood flow (rCBV) (2.240 ml/100 g, 0.844, 87.8%, and 75.9%, respectively), mean kurtosis (MK) (0.471, 0.873, 92.7%, and 79.3%), and water molecular diffusion heterogeneity index (α) (1.064, 0.847, 79.3% and 78.0%) for glioma grading. There were positive correlations between rCBV and MK and the tumor grades and negative correlations between α and the tumor grades ($p < 0.01$). The parameter of α yielded a diagnostic accuracy of 85.3%, the combination of MK and α yielded a diagnostic accuracy of 89.7%, while the combination of rCBV, MK, and α were more accurate (94.2%) in predicting tumor grade.

Conclusion: The most accurate parameters were rCBV, MK, and α in dynamic susceptibility-weighted contrast, diffusion kurtosis imaging, and Multi-b diffusion-weighted imaging for glioma grading, respectively. Multiparametric MRI can increase the accuracy of glioma grading.

Keywords: Perfusion; Diffusion; Magnetic resonance imaging; Glioma; Tumor grading.

Abbreviations: AUC area under the receiver operating characteristic curve, **CNAWM** contralateral normal appearing white matter, **D** low diffusion coefficient, **D*** fast diffusion coefficient, **Da** axial diffusion coefficient, **DDC** distributed diffusion coefficient, **DKI** diffusion kurtosis imaging, **Dr** radial diffusion coefficient, **DSC** dynamic susceptibility-weighted contrast, **f** fraction of fast ADC, **FA** fractional anisotropy, **FAK** fractional anisotropy kurtosis, **HGG** high-grade glioma, **IDH** Isocitrate dehydrogenase, **IVIM DWI** intravoxel incoherent motion diffusion-weighted imaging, **Ka** axial kurtosis, **Kr** radial kurtosis, **LGG** low-grade glioma, **MADC** multi-component apparent diffusion coefficient, **MD** mean diffusion, **MK** mean kurtosis, **MTT** mean transmit time, **rCBF** relative cerebral blood flow, **rCBV** relative cerebral blood volume, **ROC** receiver operating characteristic, **ROI** region of interest, **sADC** standard apparent diffusion coefficient, **TTP** time to peak, **WHO** World Health Organization, α water molecular diffusion heterogeneity index

INTRODUCTION

Glioma is the most common primary malignant tumor in the brain and is classified into four grades. Grade I astrocytomas have a different enhancement and/or vascularity pattern and do not follow the path of low-grade astrocytoma (grade II), which progresses to anaplastic (grade III) and finally to glioblastoma (grade IV) (1). Surgical resection is the recommended treatment for low-grade glioma (LGG), whereas adjuvant chemo- and radiotherapy after resection have been shown to produce benefits in high-grade glioma (HGG) patients (2,3). Accurately identifying and grading glioma before surgery is important for determining the appropriate treatment and evaluating the prognosis. Histopathological analysis is the current gold standard for glioma

Acad Radiol 2020; ■:1–10

From the Department of Radiology, Xinqiao Hospital, Army Medical University, Chong Qing 400037, People's Republic of China (L.Z., L.-q.Y., L.W., J.-h.H., D.Z.); Department of Neurosurgery, Xinqiao Hospital, Army Medical University, Chong Qing, People's Republic of China (S.-q.L., Q.-r.L.); Department of Pathology, Xinqiao Hospital, Army Medical University, Chong Qing, People's Republic of China (J.-p.X.); Research Service Office, Xinqiao Hospital, Army Medical University, Chong Qing, People's Republic of China (R.-f.X.). Received February 7, 2020; revised March 22, 2020; accepted March 22, 2020. **Address correspondence to:** D.Z. e-mail: zhangdongxqyy@163.com

[1] These authors contributed equally to this work.

https://doi.org/10.1016/j.acra.2020.03.035

grading; however, this can only be achieved by invasive stereotactic biopsy or surgical resection, posing a relevant additional risk to patients (4). Moreover, this approach is prone to sampling error and cannot be applied to tumors located in inaccessible brain regions, potentially resulting in inaccurate grading (5). A noninvasive method that allows accurate assessment of tumor grade is highly desirable and can overcome these limitations.

Magnetic resonance imaging (MRI) plays an important role in preoperative grading and therapy optimization (6). However, conventional MRI (cMRI) provides unsatisfactory accuracy for glioma grading. Advanced MR imaging techniques, including diffusion imaging, perfusion imaging, and spectroscopy imaging, etc., can provide additional functional information on tumor tissue in addition to morphological imaging (7–9). Tissue organization, including cell density and necrosis, can be visualized by multiple diffusion-weighted imaging (DWI) signal models. Diffusion kurtosis imaging (DKI) can be proposed to characterize the non-Gaussian water diffusion (restricted and hindered diffusion) behavior in neural tissues. Different models can be applied to multi-b value DWI (Multi-b DWI) including mono-exponential, bi-exponential, and stretched exponential models, among which bi-exponential model have been widely used in research, it can simultaneously provide diffusion and perfusion information on tumor cellularity and microcirculation without requiring a contrast agent. The water molecular diffusion heterogeneity index (α) of stretched exponential model reflected the tissue complexity by describing the heterogeneity of the diffusion rate in voxel (6). The lower the α value is, the more complex the lesion is (6). Clinically, the most commonly used perfusion MRI technique is dynamic susceptibility-weighted contrast-enhanced imaging (DSC), which can provide information on endothelial cell proliferation and neovascularization (10,11). DSC can also provide information about the size and density of normal vessels supplying neoplasms. An example is a non-enhancing glioma with elevated relative cerebral blood volume (rCBV). Various advanced MR techniques have been applied to glioma grading, meanwhile, combining different technologies has been shown to provide complementary information and can be used to obtain more comprehensive anatomical, physiological, and functional information on gliomas (12–23). This provides a better basis for accurate classification of preoperative glioma.

To our knowledge, there are few studies in the literature combining cMRI with diffusion and perfusion techniques to distinguish glioma grading. The aim of this study was to evaluate the diagnostic value and accuracy of cMRI, DSC, and multiple DWI signal models including DKI, mono-exponential, bi-exponential and stretched exponential models for preoperative glioma grading and to examine whether grading can be improved by a multimodal approach.

MATERIALS AND METHODS

Inclusion and Exclusion Criteria of Patients

This single-center retrospective study was approved by the Ethics Committee of our hospital, and informed consent was obtained from all participants.

The inclusion criteria were as follows:

- aged from 18–80 years;
- glioma confirmed pathologically;
- underwent surgery within 7 d of MR scan.

The exclusion criteria were as follows:

- intracranial lesion without operation;
- determined not to be a glioma based on pathological evaluation;
- corticosteroid therapy or chemoradiotherapy before multi-parametric MR;
- unsatisfactory image quality.

Initially, 102 patients were enrolled in this study; however, 32 subjects were excluded due to conditions specified in the criteria (Fig. 1).

Pathology

All tissues obtained from surgery were classified and graded according to the 2016 World Health Organization guidelines with standard hematoxylin-eosin staining (1). Grade II was considered LGG, whereas grades III and IV were considered HGG.

MR Protocol

Patients were examined with a 1.5T scanner (Signa Excite HDx; GE Healthcare, Milwaukee, WI) using an 8-channel

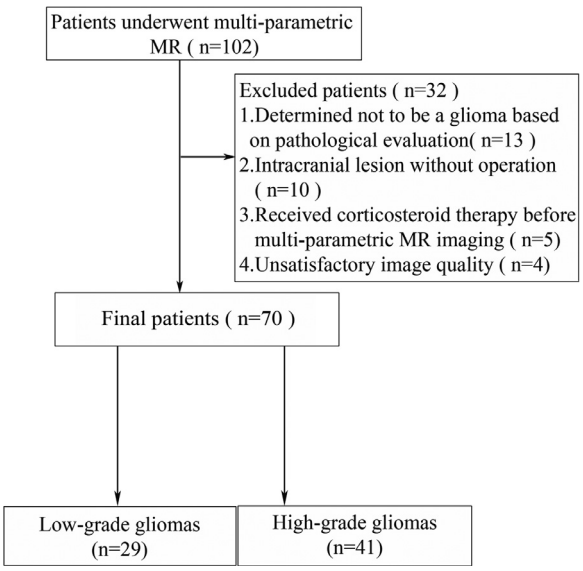

Fig. 1. Flow diagram of the patient selection process.

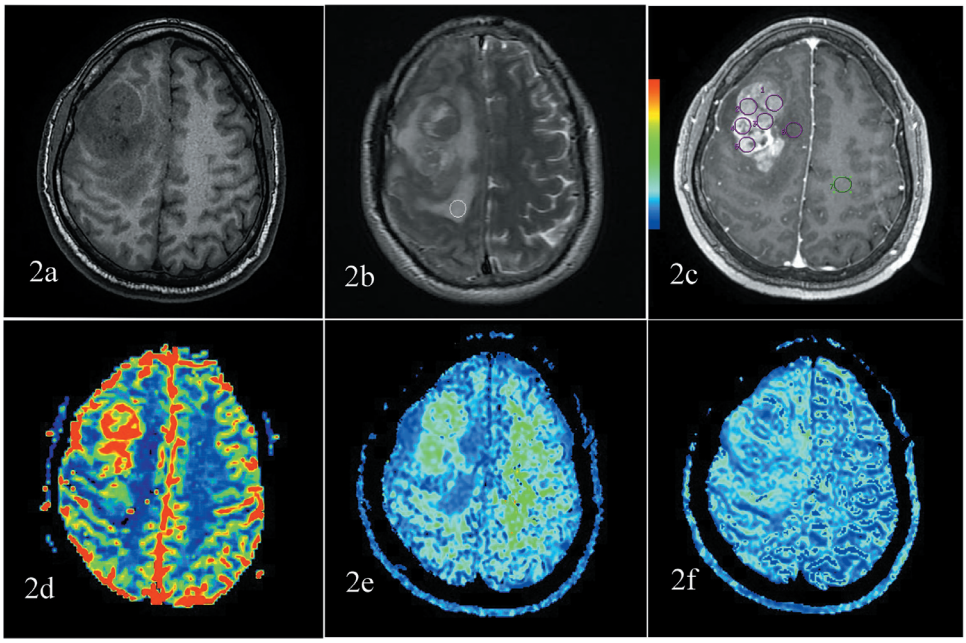

Fig. 2. A 41-year-old male patient with glioblastoma multiforme (WHO grade IV) in the right frontal lobe. The solid tumor components and peritumoral edema showed hypointense signals on T1WI (a), hyperintense signals on T2WI (b). Heterogeneous enhancement and placement of ROIs was noted on the postgadolinium T1WI (c), the tumor lesion area ROI (the purple circle, ROI 1–5), peritumoral edema ROI (ROI 6) and the contralateral normal-appearing white matter ROI (the green circle, ROI 7). The increased normalized rCBV (4.3 ml/100 g), increased normalized MK (0.9) and dsecreased normalized α (1.0) was found on rCBV map (d), MK map (e) and α map(f), respectively. MK, mean kurtosis; ROI, region of interest; rCBV, relative cerebral blood volume; WHO, World Health Organization.

phased-array head coil, and imaging sequences, respective parameters and the signal equations for multiple DWI signal models and DSC are summarized in the *Supplemental Material*. Conventional imaging, Multi-b DWI and DKI sequences were acquired before the injection of contrast. After the injection of 0.1 mmol/kg gadobenate dimeglumine, DSC sequences and conventional T1 sequences were performed. To solve the problem of the contrast leakage in DSC, we made the preload-leakage correction, in which approximately 2 ml of contrast agent was administered approximately 2 minutes before DSC imaging was performed.

Image Analysis

All multiparametric MR data were analyzed and processed on an ADW4.6 work station (Function tool; GE Healthcare). cMRIs were used to assess glioma characteristics (e.g., location, homogeneity, borders, and edema), and were carefully reviewed to determine the solid part of each tumor, peritumoral edema, and contralateral normal-appearing white matter (CNAWM).

Tumor homogeneity: the tumor MR signals were uniformly identified as homogeneous, whereas the tumor MR signals inhomogeneity (e.g., cystic, necrotic, or calcified large vessels, and hemorrhagic areas) was defined as heterogeneous.

Tumor borders were classified as sharp or indistinct. If the lesion had marked enhancement, the border was easily confirmed on T1-weighted imaging (T1WI) enhanced imaging. For tumors with no obvious enhancement, the border was confirmed on the basis of T2-weighted imaging (T2WI) and fluid attenuated inversion recovery (FLAIR) sequences, and relatively decreased signal intensity on T2WI or FLAIR was regarded as tumor area rather than edema.

Edema was defined as a nonenhanced area on contrast-enhanced T1WI and higher signal outside the tumoral solid area on T2WI and FLAIR (14).

Next, two observers placed a freehand region of interest (ROI) over the peritumoral edema to cover the highest signal intensity on T2WI or FLAIR image distance beyond the edge of the tumor (Fig. 2a). Five freehand round ROIs (Fig. 2c) on the tumor lesion area were placed without overlap, and the freehand median values of the five ROIs were selected for analysis (14,18). Regarding the tumor lesion area: enhanced tumors were delineated to cover as much of the solid part of the tumor as possible in obviously enhanced lesions on conventional three-dimensional fast spoiled gradient-echo (3D-FSPGR+C) images, while the nonenhanced tumors were delineated to cover the highest signal intensity region of the tumor on T2WI or FLAIR images. ROI selection should avoid cystic, necrotic, or calcified large vessels and hemorrhagic areas. For CNAWM, standardized ROIs (the same sizes as the lesion ROIs) were placed in the centrum semiovale (Fig. 2c). ROIs were copied to the Multi-b DWI, DSC, and DKI parameter maps after coregistration with the anatomical images.

Multi-b DWI, DKI, and DSC data were analyzed using the MADC, DKI, and a single-compartment model of an automated arterial input function of the brain perfusion

program. The mathematical correction of the time-concentration curves was performed using the BrainAIF software (Function tool, ADW4.6 work station, GE Healthcare) in DSC analysis. First, the head motion was corrected, and the threshold was then adjusted to remove the background noise, yielding a pseudo-color map of each parameter. For DSC, relative cerebral blood flow (rCBF), rCBV, mean transmit time (MTT), and time to peak (TTP) were automatically generated. For Multi-b DWI, standard apparent diffusion coefficient (sADC) was obtained based on mono-exponential model, slow diffusion coefficient (D), fast diffusion coefficient (D*) and fraction of fast ADC (f) were estimated using the bi-exponential model, distributed diffusion coefficient (DDC) and water molecular diffusion heterogeneity index (α) were calculated with stretched exponential model. For DKI, fractional anisotropy (FA), mean diffusion (MD), axial diffusion coefficient (Da), radial diffusion coefficient (Dr), FA kurtosis (FAK), mean kurtosis (MK), axial kurtosis (Ka), and radial kurtosis (Kr) were automatically generated. After the placement of ROIs on the parameter maps, the value of the previously mentioned parameters were automatically available. All quantitative parameters extracted from the tumor ROIs were normalized as follows: lesion area and/or CNAWM, which was used to eliminate whole-brain interindividual variations (15,23).

Statistical Analysis

Statistical analysis was performed using SPSS v.24.0 software (SPSS Inc., Chicago, IL). Data are expressed as the mean ± standard deviation. p values <0.05 were considered statistically significant for all tests. One-way analysis of variance was used to compare normalized lesion areas, edema, and CNAWM values of DSC, DKI and Multi-b DWI parameters between LGG and HGG, and an independent-samples t test was used to compare normalized lesion areas for all grades of glioma (II vs. III, II vs. IV, III vs. IV). A receiver operating characteristic (ROC) curve analysis was performed to determine the optimal thresholds for glioma grading by each normalized parameter. Additionally, sensitivity, specificity, and area under the curve (AUC) for glioma grading were calculated in each case. Relationships between each normalized lesion area parameter and tumor grade were analyzed with Spearman's correlation. A binary logistic regression analysis was conducted to evaluate the diagnostic accuracy of multi-parametric MR for glioma grading.

RESULTS

Patient Population and Groups

Among the 70 patients, 61 cases underwent total resection of tumor lesions and nine cases underwent partial resection of tumor lesions. Seventy histologically confirmed 29 LGG and 41 HGG cases were selected, as follows: grade II: two cases of astrocytoma with isocitrate dehydrogenase (IDH) mutation, 27 cases of diffuse astrocytoma (25 cases with IDH mutation and two cases without this mutation), grade III: 25 cases of anaplastic astrocytoma (10 cases with IDH mutation and 15 cases without this mutation), and 16 cases of grade IV: glioblastoma (three cases with IDH mutation and 13 cases without this mutation). The clinical, histological, and cMRI characteristics are summarized in Table 1. The 41 patients with HGG were older (LGG, 42 ± 8 years, and HGG, 49 ± 12 years; $p = 0.009$) and demonstrated more indistinct margins (LGG, 12/29; HGG, 24/41) than those with LGG. The LGGs were more likely to occur in the frontal lobes, whereas the HGGs were more likely to occur in the temporal and frontal lobes. Examples of HGG and LGG are provided in Figs. 2a–e and 3a–e, respectively (Fig. 3).

TABLE 1. The Main Clinical and cMRI Features in Gliomas (Between LGG and HGG)

	LGG (n = 29)	HGG (n = 41)	p Value
Sex (male/female)	15/14	20/21	0.967
Age (yr)	42 ± 8	49 ± 12	0.009*
Location			0.052
Frontal lobe	18 (26%)	12 (17%)	
Parietal lobe	2 (3%)	5 (7%)	
Temporal lobe	4 (6%)	15 (21%)	
Occipital lobe	2 (3%)	4 (6%)	
Insular lobe	2 (3%)	1 (1%)	
Others	1 (1%)	4 (6%)	
Homogeneity			0.138
Homogeneous	18 (26%)	18 (26%)	
Heterogeneous	11 (15%)	23 (33%)	
Edema			0.203
Presence	23 (33%)	37 (53%)	
Absence	6 (8%)	4 (6%)	
Borders			0.994
Sharp	17 (24%)	17 (24%)	
Indistinct	12 (17%)	24 (35%)	
Contrast enhancement			0.000*
No	21 (30%)	4 (6%)	
Yes	8 (11%)	37 (53%)	
Histology			
Grade II astrocytomas	29 (100%)	0	
Grade III astrocytomas	0	25 (61%)	
Grade IV glioblastomas	0	16 (39%)	

cMRI, conventional MRI; HGG; high-grade glioma; LGG, low-grade glioma.

Data are numbers (%) unless otherwise indicated.

* $p < 0.01$.

Comparison of DSC and Multiple DWI Signal Models Metrics Between LGG and HGG as well as Among All Grades of Glioma

DSC

The mean values of the normalized rCBF and rCBV were significantly lower for LGG than HGG in the lesion area ($p < 0.050$), and the mean value of normalized MTT was lower for LGG than HGG in the lesion area ($p < 0.050$).

TABLE 2. Comparison of DSC, DKI and Multi-b DWI Parameters Values Between LGG (n = 29) and HGG (n = 41) in Gliomas

Parameters		Tumor Lesion Area			Edema			CNAWM		
		LGG	HGG	p_1	LGG	HGG	p_2	LGG	HGG	p_3
DSC	rCBF	**2.7 ± 2.5**	**5.2 ± 3.9**	**0.003**†	11.3 ± 8.2	11 ± 8.8	0.885	8.3 ± 4.5	7.1 ± 3.7	0.228
	rCBV	**2.0 ± 1.5**	**5.2 ± 3.7**	**0.000**†	1.2 ± 0.8	1.3 ± 1.1	0.762	1.0 ± 0.5	0.8 ± 0.4	0.095
	MTT	**0.9 ± 0.2**	**1.1 ± 0.4**	**0.039***	7.1 ± 1.6	7.8 ± 2.4	0.175	7.7 ± 2.2	7. ± 1.6	0.474
	TTP	1.0 ± 0.1	1.0 ± 0.1	0.254	**20.4 ± 3.7**	**23.2 ± 5.8**	**0.027***	21.1 ± 4.1	23.2 ± 6.1	0.105
DKI	FA	0.4 ± 0.1	0.5 ± 0.2	0.059	0.3 ± 0.1	0.2 ± 0.1	0.657	0.5 ± 0.1	0.5 ± 0.1	0.916
	MD	**1.9 ± 0.6**	**1.5 ± 0.5**	**0.011***	1.3 ± 0.5	1.5 ± 0.4	0.078	0.8 ± 0.2	0.8 ± 0.1	0.051
	Da	**1.4 ± 0.4**	**1.2 ± 0.4**	**0.016***	**1.6 ± 0.5**	**1.9 ± 0.4**	**0.034***	**1.2 ± 0.2**	**1.3 ± 0.2**	**0.034***
	Dr	**2.3 ± 0.8**	**1.9 ± 0.7**	**0.014***	1.2 ± 0.5	1.3 ± 0.4	0.189	0.6 ± 0.1	0.6 ± 0.1	0.102
	FAK	**1.0 ± 0.2**	**0.8 ± 0.3**	**0.001**†	0.4 ± 0.1	0.4 ± 0.1	0.146	0.5 ± 0.1	0.5 ± 0.1	0.478
	MK	**0.4 ± 0.2**	**0.7 ± 0.2**	**0.000**†	0.6 ± 0.2	0.5 ± 0.2	0.343	1.1 ± 0.1	1.0 ± 0.1	0.064
	Ka	**0.6 ± 0.2**	**0.9 ± 0.2**	**0.000**†	0.6 ± 0.2	0.5 ± 0.1	0.161	0.9 ± 0.1	0.9 ± 0.1	0.058
	Kr	**0.3 ± 0.1**	**0.5 ± 0.1**	**0.000**†	0.6 ± 0.3	0.6 ± 0.2	0.510	1.3 ± 0.2	1.2 ± 0.2	0.181
Multi-b DWI	sADC	**2.1 ± 0.5**	**1.6 ± 0.4**	**0.000**†	1.3 ± 0.4	1.3 ± 0.3	0.747	0.7 ± 0.0	0.7 ± 0.0	0.147
	D	**4.8 ± 2.6**	**3.2 ± 1.2**	**0.001**†	0.7 ± 0.3	0.7 ± 0.3	0.915	0.3 ± 0.1	0.2 ± 0.1	0.320
	D*	1.8 ± 1.9	1.1 ± 1.3	0.052	33.7 ± 20.5	31.1 ± 26.7	0.655	29.4 ± 15.2	30.3 ± 15.3	0.809
	f	0.9 ± 0.3	1.0 ± 0.4	0.487	0.4 ± 0.1	0.4 ± 0.2	0.328	0.4 ± 0.1	0.4 ± 0.1	0.627
	DDC	**2.3 ± 0.6**	**1.8 ± 0.5**	**0.000**†	1.3 ± 0.5	1.4 ± 0.3	0.726	**0.7 ± 0.0**	**0.7 ± 0.0**	**0.049***
	α	**1.1 ± 0.1**	**1.0 ± 0.1**	**0.000**†	0.9 ± 0.0	0.9 ± 0.0	0.508	**0.8 ± 0.0**	**0.8 ± 0.0**	**0.020***

α, water molecular diffusion heterogeneity index; D, slow diffusion coefficient; D*, fast diffusion coefficient; Da, axial diffusion; DDC, distributed diffusion coefficient; Dr, radial diffusion; f, fraction of fast ADC; FA, fractional anisotropy; FAK, fractional anisotropy kurtosis; Ka, axial kurtosis; Kr, radial kurtosis; MD, mean diffusion; MK, mean kurtosis; MTT, mean transmit time; rCBF, relative cerebral blood flow; rCBV, relative cerebral blood volume; sADC, standard apparent diffusion coefficient; TTP, relative time to peak.

p_1, analysis of variance in lesion area.

p_2, analysis of variance in edema.

p_3, analysis of variance in CNAWM.

The unit of parameters: rCBF (ml/100 g/min); rCBV (ml/100 g); MTT (s); TTP (s); MD (μm^2/ms); Da (μm^2/ms); Dr (μm^2/ms); sADC ($\times 10^{-3}$ mm^2/s); D ($\times 10^{-3}$ mm^2/s); D* ($\times 10^{-3}$ mm^2/s); DDC ($\times 10^{-3}$ mm^2/s).

* $p < 0.05$.

† $p < 0.01$.

However, the mean normalized TTP values of the lesion area did not differ between LGG and HGG ($p > 0.050$). The mean TTP value in cases of peritumoral edema was lower for LGG than HGG ($p < 0.050$). There were no significant differences in rCBF, rCBV, MTT, and TTP in CNAWM between LGG and HGG ($p > 0.050$; Table 2).

The mean values of the normalized rCBF and rCBV values were significantly lower for grade II glioma than grade III and IV glioma in the lesion area ($p < 0.050$), whereas compared to grade II glioma, the MTT value was significantly higher in grade IV glioma ($p < 0.050$; Table 3).

Multiple DWI Signal Models

DKI

In the lesion area, the mean values of the normalized MK, Ka, and Kr were lower for LGG than HGG ($p < 0.050$), whereas the opposite trend was observed for the mean values of the normalized MD, Da, Dr, and FAK ($p < 0.050$). The mean Da value in cases of peritumoral edema and CNAWM was lower in LGG than in HGG ($p < 0.05$; Table 2).

The mean values of the normalized MK and Kr values were significantly lower for grade II glioma than grade III and IV glioma ($p < 0.050$) and were significantly lower for grade III glioma than grade IV glioma ($p < 0.050$). The mean values of the normalized Da and FAK values were significantly higher, whereas the Ka values were significantly lower for grade II glioma than grade III and IV glioma in the lesion area ($p < 0.050$). In grade IV glioma, compared to grade II glioma, the MD and Dr values were significantly lower, and the FA values were significantly higher ($p < 0.050$; Table 3).

Remaining DWI Signal Models

The mean values of the normalized sADC, D, DDC, and α were higher for LGG than HGG in the lesion area ($p < 0.050$). The mean values of DDC and α were slightly lower in LGG than HGG in CNAWM ($p < 0.050$; Table 2).

The mean values of the normalized sADC values were significantly higher for grade II glioma than grade III and IV glioma ($p < 0.050$) and were significantly higher for grade III glioma than for grade IV glioma ($p < 0.050$). The mean values of the normalized D, DDC, and α values were significantly higher for grade II glioma than for grade III and IV glioma in the lesion area ($p < 0.050$; Table 3).

TABLE 3. Comparison of DSC, DKI, and Multi-b DWI Parameter Values in the Normalized Lesion Area Across All Grades of Glioma

Parameters		Ⅱ (n = 29)	Ⅲ((n = 25)	Ⅳ (n = 16)	Ⅱ &Ⅲ (p)	Ⅱ &Ⅳ (p)	Ⅲ &Ⅳ (p)
DSC	rCBF	2.7 ± 2.5	4.7 ± 2.8	6.0 ± 5.1	**0.008**†	**0.006**†	0.301
	rCBV	2.0 ± 1.5	4.7 ± 2.9	6.1 ± 4.8	**0.000**†	**0.000**†	0.229
	MTT	0.9 ± 0.2	1.0 ± 0.3	1.2 ± 0.5	0.117	**0.022***	0.255
	TTP	1.0 ± 0.1	1.0 ± 0.1	1.0 ± 0.1	0.523	0.154	0.395
DKI	FA	0.4 ± 0.1	0.4 ± 0.2	0.5 ± 0.2	0.303	**0.009**†	-0.105
	MD	1.9 ± 0.6	1.6 ± 0.5	1.4 ± 0.5	0.066	**0.017***	0.308
	Da	1.4 ± 0.4	1.2 ± 0.3	1.2 ± 0.5	**0.049***	**0.045***	0.567
	Dr	2.3 ± 0.8	2.0 ± 0.7	1.8 ± 0.7	0.093	**0.015***	0.244
	FAK	1.0 ± 0.2	0.8 ± 0.3	0.8 ± 0.2	**0.004**†	**0.005**†	0.985
	MK	0.4 ± 0.2	0.6 ± 0.2	0.8 ± 0.2	**0.000**†	**0.000**†	**0.007**†
	Ka	0.6 ± 0.2	0.8 ± 0.2	0.9 ± 0.2	**0.000**†	**0.000**†	0.295
	Kr	0.3 ± 0.1	0.5 ± 0.1	0.6 ± 0.1	**0.000**†	**0.000**†	**0.015***
Multi-b DWI	sADC	2.1 ± 0.5	1.7 ± 0.4	1.4 ± 0.4	**0.011***	**0.000**†	**0.038***
	D	4.8 ± 2.6	3.3 ± 1.4	3.0 ± 1.0	**0.013***	**0.011***	0.443
	D*	1.8 ± 1.9	1.1 ± 1.6	1.0 ± 0.7	0.144	0.099	0.786
	f	0.9 ± 0.3	1.0 ± 0.4	0.9 ± 0.3	0.268	0.835	0.274
	DDC	2.3 ± 0.6	1.9 ± 0.5	1.6 ± 0.5	**0.017***	**0.000**†	0.058
	α	1.1 ± 0.1	1.0 ± 0.1	1.0 ± 0.6	**0.000**†	**0.000**†	0.994

α, water molecular diffusion heterogeneity index; D, slow diffusion coefficient; D*, fast diffusion coefficient; Da, axial diffusion; DDC, distributed diffusion coefficient; Dr, radial diffusion; f, fraction of fast ADC; FA, fractional anisotropy; FAK, fractional anisotropy kurtosis; Ka, axial kurtosis; Kr, radial kurtosis; MD, mean diffusion; MK, mean kurtosis; MTT, mean transmit time; rCBF, relative cerebral blood flow; rCBV, relative cerebral blood volume; sADC, standard apparent diffusion coefficient; TTP, relative time to peak.

The unit of parameters: rCBF (ml/100 g/min); rCBV (ml/100 g); MTT (s); TTP (s); MD (μm^2/ms); Da (μm^2/ms); Dr (μm^2/ms); sADC ($\times 10^{-3}$ mm^2/s); D ($\times 10^{-3}$ mm^2/s); D* ($\times 10^{-3}$ mm^2/s); DDC ($\times 10^{-3}$ mm^2/s).

* $p < 0.05$.

† $p < 0.01$.

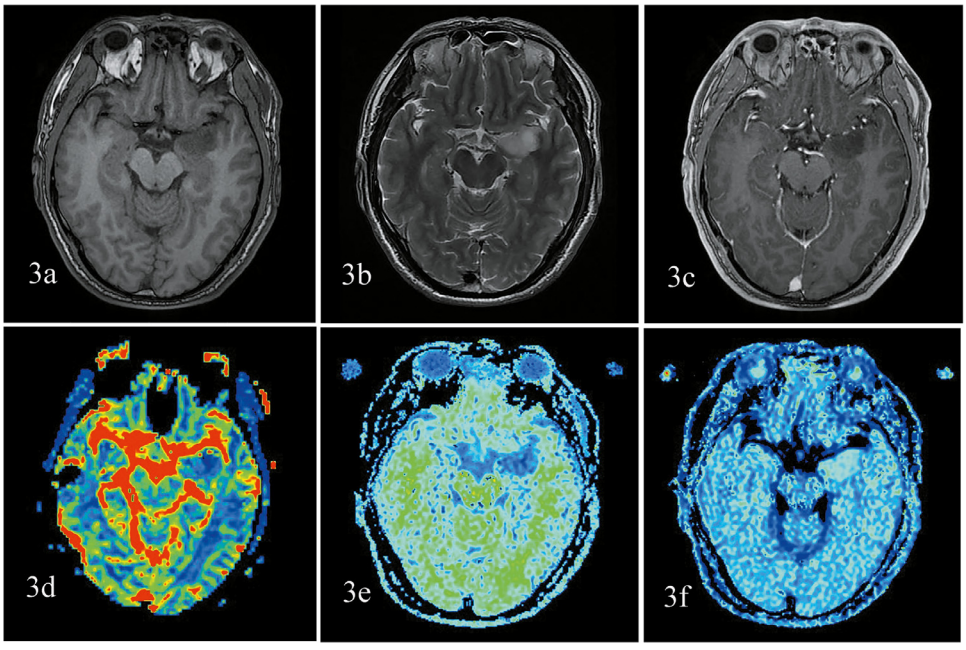

Fig. 3. A 53-year-old male patient with diffuse astrocytoma (WHO grade II) in the left temporal lobe. The solid tumor components showed hypointense signal on T1WI (a), hyperintense signal on T2WI (b), no obvious tumor peripheral edema (a, b) and no enhancement was observed on the postgadolinium T1WI (c). no obviously increased normalized rCBV(1.3 ml/100 g), decreased normalized MK (0.3) and increased normalized α (1.2) map was found on rCBV map (d), MK map (e) and α map (f), respectively. MK, mean kurtosis; rCBV, relative cerebral blood volume; WHO, World Health Organization.

TABLE 4. Correlations Between Glioma Grade and Parameters of the Tumor Lesion Area

	Parameters	Spearman Correlation Coefficient	*p* Value
DSC	rCBF	**0.369**	**0.002**†
	rCBV	**0.488**	**0.000**†
	MTT	**0.293**	**0.014***
	TTP	0.174	0.150
DKI	FA	**0.309**	**0.009**†
	MD	**−0.317**	**0.007**†
	Da	**−0.282**	**0.018***
	Dr	**−0.317**	**0.008**†
	FAK	**−0.343**	**0.004**†
	MK	**0.642**	**0.000**†
	Ka	**0.521**	**0.000**†
	Kr	**0.622**	**0.000**†
Multi-b DWI	sADC	**−0.475**	**0.000**†
	D	**−0.366**	**0.002**†
	D*	−0.218	0.070
	f	0.007	0.957
	DDC	**−0.455**	**0.000**†
	α	**−0.501**	**0.000**†

α, water molecular diffusion heterogeneity index; D, slow diffusion coefficient; D*, fast diffusion coefficient; Da, axial diffusion; DDC, distributed diffusion coefficient; Dr, radial diffusion; f, fraction of fast ADC; FA, fractional anisotropy; FAK, fractional anisotropy kurtosis; Ka, axial kurtosis; Kr, radial kurtosis; MD, mean diffusion; MK, mean kurtosis; MTT, mean transmit time; rCBF, relative cerebral blood flow; rCBV, relative cerebral blood volume; sADC, standard apparent diffusion coefficient; TTP, relative time to peak.

* Correlation is significant at the 0.05 level (2-tailed).

† correlation is significant at the 0.01 level (2-tailed).

Correlations Between DSC and Multiple DWI Signal Models Parameter Values and Glioma Grade

There were significant positive correlations between the normalized rCBF, rCBV, MTT, FA, MK, Ka, and Kr values and tumor grades ($p < 0.010$), whereas negative correlations were observed between MD, Da, Dr, FAK, sADC, D, D∗, DDC, and α values and tumor grades ($p < 0.010$; Table 4).

ROC Analysis of the Normalized DSC and Multiple DWI Signal Models Parameters for Glioma Grading

An ROC analysis was performed to determine the optimal thresholds, AUC, sensitivity, and specificity for differentiating the performance of the normalized DSC, DKI, and Multi-b DWI parameters regarding the diagnosis of LGG and HGG (Table 5). The normalized mean rCBV (2.240 ml/100 g, 0.844, 87.8% and 75.9% for the optimal threshold, AUC, sensitivity, and specificity, respectively), MK (0.471, 0.873, 92.7% and 79.3%) and α (1.064, 0.847, 79.3% and 78.0%) showed the best diagnostic performance for identifying the glioma grade (Fig. 4).

Diagnostic Accuracy of Multiparametric MR in Glioma Grading

When we compared the multiparametric MR parameters, including the parameters of normalized rCBV, MK, and α in DSC, DKI, and Multi-b DWI, respectively. The α parameter from Multi-b DWI (85.3%) showed the best diagnostic accuracy relative to the other modalities, followed by the MK parameter from DKI (83.4%) and the rCBV parameter from DSC (79.6%) for glioma grading. The diagnostic accuracy was 89.7% for the combination of the MK parameter from DKI and the α parameter from Multi-b DWI, followed by the rCBV parameter from DSC. The α parameter from Multi-b DWI (86.1%) and the rCBV parameter from DSC and the MK parameter from DKI (81.9%). The combination of the three advanced MR parameters (rCBV, MK, and α) showed the highest accuracy for predicting tumor grade (the diagnostic accuracy of the statistical analysis was 94.2%).

DISCUSSION

The present study demonstrated that the most accurate parameters were rCBV, MK, and α in DSC, DKI, and Multi-b DWI for glioma grading, respectively. Multiparametric MR can increase the accuracy of glioma grading. Our results provide a basis for more accurately grading of gliomas, which will facilitate better treatment decisions for individual patients.

Application Value of DSC in Grading Gliomas

DSC quantitatively reflects tumor microvessel density, vascular properties and distribution and can be used to evaluate the extent of tumor neoangiogenesis and invasion of surrounding tissue by measuring rCBV and rCBF, which have been found to be highly accurate predictors of tumor grade (18,24–26). HGG exhibits high perfusion in terms of high CBV and CBF values in the tumor area due to abundant angiogenesis. We found that the mean values of the normalized rCBF and rCBV values were significantly lower for grade II glioma than for grade III and IV glioma in the lesion area ($p < 0.050$), which was in agreement with previous studies. Thus, rCBF and rCBV best reflect the hemodynamic response in glioma, which can be used to evaluate the pathological grade of glioma before surgery. The results obtained here were similar to previous studies (27–29). However, the accuracy, sensitivity and specificity were lower than those in earlier reports, possibly because our study included more cases ($n = 70$) and adopted different methods for ROI selection.

Application Value of DKI in Grading Gliomas

DKI was proposed to characterize the non-Gaussian water diffusion (restricted and hindered diffusion) behavior in neural tissues (30). HGG has greater structural complexity and

TABLE 5. Threshold Values for Multiple Parameters for Differentiating LGG From HGG

	Parameters	Threshold	AUC	Sensitivity (%)	Specificity (%)
DSC	rCBF	2.347	0.767	80.5	69.0
	rCBV	**2.240**	**0.844**	**87.8**	**75.9**
	MTT	0.841	0.659	80.5	48.3
	TTP	0.964	0.555	53.7	65.5
DKI	FA	0.422	0.604	46.3	82.8
	MD	1.443	0.714	89.7	56.1
	Da	1.182	0.714	72.4	68.3
	Dr	1.880	0.710	79.3	65.9
	FAK	0.918	0.738	69.0	70.7
	MK	**0.471**	**0.873**	**92.7**	**79.3**
	Ka	0.642	0.841	90.2	69.0
	Kr	0.339	0.871	90.2	82.8
Multi-b DWI	sADC	1.622	0.774	93.1	63.4
	D	3.585	0.699	69.0	75.6
	D*	1.648	0.680	79.3	56.1
	f	1.150	0.526	31.7	82.8
	DDC	1.813	0.765	93.1	63.4
	α	**1.064**	**0.847**	**79.3**	**78.0**

α, water molecular diffusion heterogeneity index; D, slow diffusion coefficient; D*, fast diffusion coefficient; Da, axial diffusion; DDC, distributed diffusion coefficient; Dr, radial diffusion; f, fraction of fast ADC; FA, fractional anisotropy; FAK, fractional anisotropy kurtosis; Ka, axial kurtosis; Kr, radial kurtosis; MD, mean diffusion; MK, mean kurtosis; MTT, mean transmit time; rCBF, relative cerebral blood flow; rCBV, relative cerebral blood volume; sADC, standard apparent diffusion coefficient; TTP, relative time to peak.

LGG-positive: MD, Da, Dr, FAK, sADC, D, D*, DDC, and α.

HGG-positive: rCBF, rCBV, rMTT, rTTP, FA, MK, Ka, Kr, and f.

The unit of parameters: rCBF (ml/100 g/min); rCBV (ml/100 g); MTT (s); TTP (s); MD (μm^2/ms); Da (μm^2/ms); Dr (μm^2/ms); sADC ($\times 10^{-3}$ mm^2/s); D ($\times 10^{-3}$ mm^2/s); D* ($\times 10^{-3}$ mm^2/s); DDC ($\times 10^{-3}$ mm^2/s).

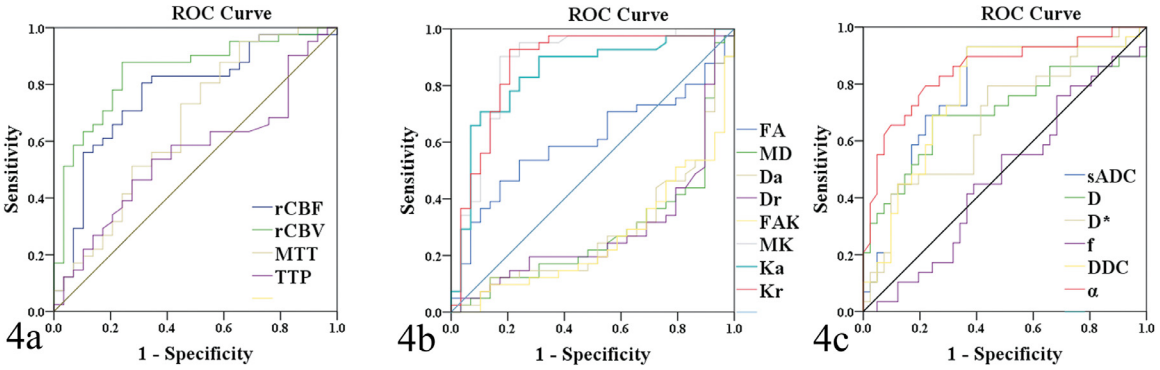

Fig. 4. ROC curves for differentiating the performance of normalized DSC (a), DKI (b) and Multi-b DWI (c) parameters in the lesion area. DKI, diffusion kurtosis imaging; DSC, dynamic susceptibility-weighted contrast; DWI, diffusion-weighted imaging; ROC, receiver operating characteristic.

heterogeneity than LGG, which increases kurtosis but decreases the diffusion range (15).

Previous reports have analyzed only one or a few DKI parameters (15,23,31), and this did not provide comprehensive information about lesions. Our study is distinguished from previous work by the fact that we selected more DKI parameters. In this study, we analyzed all available DKI parameters and compared these metrics between LGG and HGG. We found that normalized kurtosis metrics in the lesion area were more useful than values that were not normalized for glioma grading. The normalized MK values showed higher values for the AUC, sensitivity, and specificity in differentiating all grades. The kurtosis metric (e.g., MK) of DKI is a promising imaging marker for the accurate identification of microstructural changes caused by increased cell proliferation and associated with higher glioma grades, which could lead to a more accurate diagnosis and optimized therapy for glioma patients.

In addition, it was interesting to note that there were significant differences in the CNAWM between the LGG and HGG groups across numerous DKI parameters, including MD, Da, MK, and Ka. This result is concordant with data from other studies (15,23,31). The reason may be that the tumor invaded and destroyed nerve fibers in local brain regions, which affected the connection of the whole-brain neural network or caused changes in the microstructure and microenvironment of brain tissue. Thus, combined with these parameters in the contralateral normal white matter area, these parameters can provide more effective imaging indicators for the early diagnosis of HGG and LGG and an improvement in the overall diagnostic efficiency.

Application Value of Remaining DWI Signal Models in Glioma Grading

Multi-b DWI can simultaneously provide diffusion and perfusion information on tumor cellularity and microcirculation without requiring the use of a contrast agent (32). Currently, Multi-b DWI has mono-exponential, bi-exponential, and stretched exponential models, among which bi-exponential models have been widely used in research. Unlike previous research reports that used only one model, we used a mono-exponential(by measuring the sADC value), a bi-exponential model (by measuring D, D^*, and f values) and a stretched exponential model (by measuring DDC and α values) for glioma grading. The resulting parameters of the three models were compared regarding their utility in differentiating LGG from HGG and differentiating across all grades of glioma. We found that the normalized f and D^* values in the lesion area did not significantly differ between LGG and HGG ($p > 0.05$), which contradicted the findings of other studies (22,33). One possible reason is that these studies used different scanning equipment and different methods for selecting ROIs as well as different b values (since a lower b value was more important for calculating pseudodiffusion, and the b value can influence the accuracy of f value measurements) (34).

Meanwhile, after comparing all the parameters of the three models, we showed that the stretched exponential model plays a potential role in glioma grading. Furthermore, our results suggested that other parameters calculated from Multi-b DWI could potentially be useful for noninvasive glioma grading.

Application Value of Multiparametric MRI in Grading Gliomas

Some studies have reported that the combination of multiparametric MR technology can improve the accuracy of glioma grading. Van Cauter S et al. (11) reported that the most accurate tumor grading can be achieved with a combination of DKI, DSC, and magnetic resonance spectrum (MRS). Another study using cMRI, DTI, DSC, and MRS concluded that combining all parameters was useful for individually classifying gliomas as low or high grade (35). For the first time, we used a combination of cMRI, DSC, and multiple DWI signal models for glioma grading. The results demonstrated that mean rCBV, MK, and α values were the best diagnostic parameters of DSC, DKI, and remaining DWI signal models, respectively, for glioma grading. Evaluations based on the combination of multiple parameter values provided a better assessment of glioma grading.

Apart from the intrinsic limits of any retrospective study, several other limitations of our study should be mentioned. First, differences between glioma subtypes were not studied because of the small sample size. Second, only the most abnormal regions within the tumor volumes were manually selected as ROIs, but not the entire tumor volume. Ideally, it would be better to select the entire tumor volume as the ROI. We will refine this in future studies. Third, the range and number of b values can affect accurate assessments of f and D∗ but there is currently no consensus on the optimal number and range of b values for Multi-b DWI. Finally, high accuracy for glioma grading reported in this study may be related to over-fitting. Ideally, a larger dataset should be studied and divided into training and testing data, so that the latter could be used to evaluate the performance of the model designed through fitting to the training data. These limitations will be considered and improved in future research work.

In conclusion, the results of this study showed that the combination of DSC, DKI, and Multi-b DWI was useful for preoperative noninvasive glioma grading and that the best diagnostic performance parameters were the mean rCBV, MK, and α, respectively. When individually comparing each modality, the parameter of α from Multi-b DWI had the best diagnostic accuracy, while combining multiple MR parameters further enhanced the diagnostic performance for glioma grading. These results provide a basis for more accurate grading glioma, which will better facilitate correct treatment decisions for individual patients.

FUNDING

This research was supported by grants from the National Science Foundation of China (grant no. 81471635); Chongqing Science & Technology Commission of China (grant no. cstc2017shmsA0896); Chongqing Science & Technology Commission of China (grant no. cstc2017jcyjBX0038); and the clinical research project of The Third Military Medical University of China (grant no. 2016YLC24).

ACKNOWLEDGMENTS

We thank AJE (http://www. aje.com, using the verification code C2A8-4423-4D02-09B7-BC0P) for editing this manuscript.

REFERENCES

1. Louis DN, Perry A, Reifenberger G, et al. The 2016 World Health Organization classification of tumors of the central nervous system: a summary. Acta Neuropathol 2016; 131(6):803–820.

2. Park JE, Kim HS, Park KJ, et al. Histogram analysis of amide proton transfer imaging to identify contrast-enhancing low-grade brain tumor that mimics high-grade tumor: increased accuracy of MR perfusion. Radiology 2015; 277(1):151–161.
3. Le Rhun E, Taillibert S, Chamberlain MC. Anaplastic glioma: current treatment and management. Expert Rev Neurother 2015; 15(6):601–620.
4. Field M, Witham TF, Flickinger JC, et al. Comprehensive assessment of hemorrhage risks and outcomes after stereotactic brain biopsy. J Neurosurg 2001; 94(4):545–551.
5. Arevalo-Perez J, Kebede AA, Peck KK, et al. Dynamic contrast-enhanced MRI in low-grade versus anaplastic oligodendrogliomas. J Neuroimaging 2016; 26(3):366–371.
6. Kao HW, Chiang SW, Chung HW, et al. Advanced MR imaging of gliomas: an update. Biomed Res Int 2013; 2013:970586.
7. Heiss WD, Raab P, Lanfermann H. Multimodality assessment of brain tumors and tumor recurrence. J Nucl Med 2011; 52(10):1585–1600.
8. Morita N, Harada M, Otsuka H, et al. Clinical application of MR spectroscopy and imaging of brain tumor. Magn Reson Med Sci 2010; 9(4):167–175.
9. Lee SK. Diffusion tensor and perfusion imaging of brain tumors in high-field MR imaging. Neuroimaging Clin N Am 2012; 22(2):123–134.
10. Cha S. Update on brain tumor imaging: from anatomy to physiology. AJNR Am J Neuroradiol 2006; 27(3):475–487.
11. Van Cauter S, De Keyzer F, Sima DM, et al. Integrating diffusion kurtosis imaging, dynamic susceptibility-weighted contrast-enhanced MRI, and short echo time chemical shift imaging for grading gliomas. Neuro-Oncology 2014; 16(7):1010–1021.
12. Kounelakis MG, Dimou IN, Zervakis ME, et al. Strengths and weaknesses of 1.5T and 3T MRS data in brain glioma classification. IEEE Trans Inf Technol Biomed 2011; 15(4):647–654.
13. McKnight TR, Smith KJ, Chu PW, et al. Choline metabolism, proliferation, and angiogenesis in nonenhancing grades 2 and 3 astrocytoma. J Magn Reson Imaging 2011; 33(4):808–816.
14. Xing Z, Yang X, She D, et al. Noninvasive assessment of IDH mutational status in World Health Organization grade II and III astrocytomas using DWI and DSC-PWI combined with conventional MR imaging. AJNR Am J Neuroradiol 2017; 38(6):1138–1144.
15. Van Cauter S, Veraart J, Sijbers J, et al. Gliomas: diffusion kurtosis MR imaging in grading. Radiology 2012; 263(2):492–501.
16. Raab P, Hattingen E, Franz K, et al. Cerebral gliomas: diffusional kurtosis imaging analysis of microstructural differences. Radiology 2010; 254 (3):876–881.
17. Han X, Suo S, Sun Y, et al. Apparent diffusion coefficient measurement in glioma: Influence of region-of-interest determination methods on apparent diffusion coefficient values, interobserver variability, time efficiency, and diagnostic ability. J Magn Reson Imaging 2017; 45(3):722–730.
18. Santarosa C, Castellano A, Conte GM, et al. Dynamic contrast-enhanced and dynamic susceptibility contrast perfusion MR imaging for glioma grading: preliminary comparison of vessel compartment and permeability parameters using hotspot and histogram analysis. Eur J Radiol 2016; 85(6):1147–1156.
19. Chawla S, Krejza J, Vossough A, et al. Differentiation between oligodendroglioma genotypes using dynamic susceptibility contrast perfusion-weighted imaging and proton MR spectroscopy. AJNR Am J Neuroradiol 2013; 34(8):1542–1549.
20. Li F, Shi W, Wang D, et al. Evaluation of histopathological changes in the microstructure at the center and periphery of glioma tumors using diffusional kurtosis imaging. Clin Neurol Neurosurg 2016; 151:120–127.
21. Li X, Zhu Y, Kang H, et al. Glioma grading by microvascular permeability parameters derived from dynamic contrast-enhanced MRI and intratumoral susceptibility signal on susceptibility weighted imaging. Cancer Imaging 2015; 15:4.
22. Hu YC, Yan LF, Wu L, et al. Intravoxel incoherent motion diffusion-weighted MR imaging of gliomas: efficacy in preoperative grading. Sci. Rep 2014; 4:7208.
23. Jiang R, Jiang J, Zhao L, et al. Diffusion kurtosis imaging can efficiently assess the glioma grade and cellular proliferation. Oncotarget 2015; 6 (39):42380–42393.
24. Sadeghi N, D'Haene N, Decaestecker C, et al. Apparent diffusion coefficient and cerebral blood volume in brain gliomas: relation to tumor cell density and tumor microvessel density based on stereotactic biopsies. AJNR Am. J. Neuroradiol 2008; 29(3):476–482.
25. Roy B, Awasthi R, Bindal A, et al. Comparative evaluation of 3-dimensional pseudo continuous arterial spin labeling with dynamic contrast-enhanced perfusion magnetic resonance imaging in grading of human glioma. J Comput Assist Tomogr 2013; 37(3):321–326.
26. Wang XC, Zhang H, Tan Y, et al. Combined value of susceptibility weighted and perfusion-weighted imaging in assessing WHO grade for brain astrocytomas. J Magn Reson Imaging 2013; 39(6):1569–1574.
27. Ma H, Wang Z, Xu K, et al. Three-dimensional arterial spin labeling imaging and dynamic susceptibility contrast perfusion-weighted imaging value in diagnosing glioma grade prior to surgery. Exp Ther Med 2017; 13(6):2691–2698.
28. Nguyen TB, Cron GO, Perdrizet K, et al. Comparison of the diagnostic accuracy of DSC- and dynamic contrast-enhanced MRI in the preoperative grading of astrocytomas. AJNR Am J Neuroradiol 2015; 36 (11):2017–2022.
29. Xiao HF, Chen ZY, Lou X, et al. Astrocytic tumour grading: a comparative study of three-dimensional pseudocontinuous arterial spin labelling, dynamic susceptibility contrast-enhanced perfusion-weighted imaging, and diffusion-weighted imaging. Eur Radiol 2015; 25(12):3340–3423.
30. Veraart J, Poot DH, Van Hecke W, et al. More accurate estimation of diffusion tensor parameters using diffusion Kurtosis imaging. Magn Reson Med 2011; 65(1):138–145.
31. Tietze A, Hansen MB, Østergaard L, et al. Mean diffusional kurtosis in patients with glioma: initial results with a fast imaging method in a clinical setting. AJNR Am J Neuroradiol 2015; 36(8):1472–1478.
32. Hu YC, Yan LF, Sun Q, et al. Comparison between ultra-high and conventional mono b-value DWI for preoperative glioma grading. Oncotarget 2017; 8(23):37884–37895.
33. Federau C, Meuli R, O'Brien K, et al. Perfusion measurement in brain gliomas with intravoxel incoherent motion MRI. AJNR Am J Neuroradiol 2014; 35(2):256–262.
34. Cohen AD, Schieke MC, Hohenwalter MD, et al. The effect of low b-values on the intravoxel incoherent motion derived pseudo diffusion parameter in liver. Magn Reson Med 2015; 73(1):306–311.
35. Roy B, Gupta RK, Maudsley AA, et al. Utility of multiparametric 3-T MRI for glioma characterization. Neuroradiology 2013; 55(5):603–613.

SUPPLEMENTARY MATERIALS

Supplementary material associated with this article can be found in the online version at doi:10.1016/j.acra.2020.03.035.